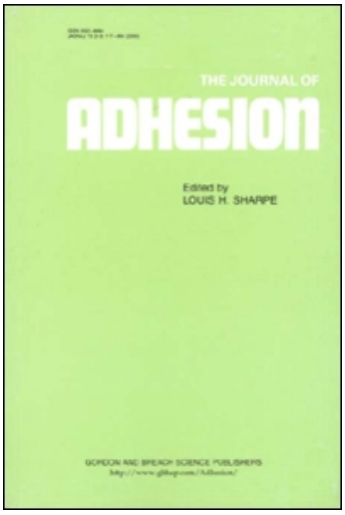

The Journal of Adhesion
Publication details, including instructions for authors and subscription information:
http://www.informaworld.com/smpp/title~content=t713453635

A Stress Analysis of Adhesive Butt Joints of Dissimilar Materials Subjected to Cleavage Loads

Y. Nakano[a]; K. Temma[b]; T. Sawa[c]
[a] Department of Mechanical Engineering, Shonan Institute of Technology, Fujisawa, Kanagawa, Japan [b] Department of Mechanical Engineering, Kisarazu National College of Technology, Kisarazu, Chiba, Japan [c] Department of Mechanical Engineering, Yamanashi University, Kofu, Yamanashi, Japan

To cite this Article Nakano, Y. , Temma, K. and Sawa, T.(1991) 'A Stress Analysis of Adhesive Butt Joints of Dissimilar Materials Subjected to Cleavage Loads', The Journal of Adhesion, 34: 1, 137 — 151
To link to this Article: DOI: 10.1080/00218469108026510
URL: http://dx.doi.org/10.1080/00218469108026510

J. Adhesion, 1991, Vol. 34, pp. 137–151
Reprints available directly from the publisher
Photocopying permitted by license only

Printed in the United Kingdom

A Stress Analysis of Adhesive Butt Joints of Dissimilar Materials Subjected to Cleavage Loads

Y. NAKANO

Department of Mechanical Engineering, Shonan Institute of Technology, Fujisawa, Kanagawa, Japan

K. TEMMA

Department of Mechanical Engineering, Kisarazu National College of Technology, Kisarazu, Chiba, Japan

T. SAWA

Department of Mechanical Engineering, Yamanashi University, Kofu, Yamanashi, Japan

(Received Aug. 27, 1990; in final form Jan. 9, 1991)

Stress distributions are examined when an adhesive butt joint, in which two thin plates made of dissimilar materials are joined, is subjected to cleavage loads. General representations of the stress and displacement fields are given using the two-dimensional theory of elasticity. The effects of the ratios of young's modulus among two adherends and an adhesive and the thickness of the adhesive on the stress distributions of the joints are clarified by numerical calculations. In addition, the stress singularity near the edge of the interface in the load application side is evaluated. For verification, the strain distributions near the interface of each adherend were measured. The analytical results are closely consistent with the experimental ones.

KEY WORDS elasticity; stress analysis; butt joint; cleavage load; stress singularity; plane stress; plane strain; dissimilar material.

1 INTRODUCTION

An adhesive bonding of structural elements has several attractive features as compared with bolted or riveted joints. For example, 1) it is not necessary to drill holes in the element to insert bolts or rivets, so that the stress will distribute more uniformly throughout the joint, 2) ease in joining the structural elements of dissimilar materials, 3) decreasing the weight of the joint is possible, 4) smoother and more aesthetic appearance of the joint is possible. Adhesive bonding has been recognized as one of the rational joining methods and is beginning to be used in the field of manufacturing.

However, enough fundamental data has not been acquired to design adhesive joints in practice, and an estimation method for the strength of adhesive joints has not been sufficiently established at present. Some remaining problems need to be solved so that adhesive joints can be used in the practical and important parts of structures with sufficient reliability. One of the most important problems is to examine the stress distribution in the joints, especially in the optimal strength design of adhesive joints.

From this point of view, some investigations have been done on the stress distributions of adhesive joints under several types of loading using experimental methods, the finite element method[1–3] and the theory of elasticity.[4–10] Most of these analytical investigations have been carried out on joints which consist of similar adherends, although it is a distinctive feature compared with conventional joining methods that joining two structural elements made of dissimilar materials is easy, as mentioned above.

This paper describes the stress distributions and the displacements of an adhesive butt joint subjected to cleavage loads in which two thin plates made of dissimilar materials are jointed.[11] In the analyses, two dissimilar adherends of the same size and the adhesive layer are modeled as finite strips. The adhesive butt joint is modeled as an elastic three-body problem. Then, using the two-dimensional theory of elasticity, the stress distributions and the displacements of each strip are analyzed subject to the boundary conditions. The effects of the ratios of Young's modulus among two dissimilar adherends and the adhesive, and the thickness of the adhesive bond, on the stress distributions are clarified by numerical calculations. Moreover, the calculated results show that the stress becomes singular at the edge of the interface, so the singular behavior near the edge of the interface is investigated to evaluate the strength of the adhesive joint. For verification, some experiments were performed and it was found that the analytical results were closely consistent with the experimental ones.

2 THEORETICAL ANALYSIS

Figure 1 shows an adhesive butt joint of two dissimilar adherends of the same size. A distributed cleavage load $\mathbf{P}_0$ acts over the distance $\mathbf{e}$ from the end of the upper and the lower surfaces of the adherends. The two adherends are replaced with the finite strips (I) and (III) and the adhesive layer with the finite strip (II). The width and the height of the strips (I) and (III) are designated by $\mathbf{2L}$ and $\mathbf{2H}_1$, respectively, and those of the strip (II) by $\mathbf{2L}$ and $\mathbf{2H}_2$, respectively. Young's modulus and Poisson's ratio of each strip are denoted as $\mathbf{E}_1$, ν_1, $\mathbf{E}$, ν_2, and $\mathbf{E}_3$, ν_3, respectively.

Boundary conditions of this adhesive butt joint are as follows. On the strip (I), i.e., the adherend (I),

$$\sigma_x^{\mathrm{I}} = \tau_{xy}^{\mathrm{I}} = 0 \quad (x = \pm L) \tag{1-a}$$

$$\sigma_y^{\mathrm{I}} = \begin{cases} P_0 & (-L \leqq x \leqq -L + e) \\ 0 & (-L + e \leqq x \leqq +L) \end{cases} \quad (y_1 = +H_1) \tag{1-b}$$

$$\tau_{xy}^{\mathrm{I}} = 0 \quad (y_1 = +H_1) \tag{1-c}$$

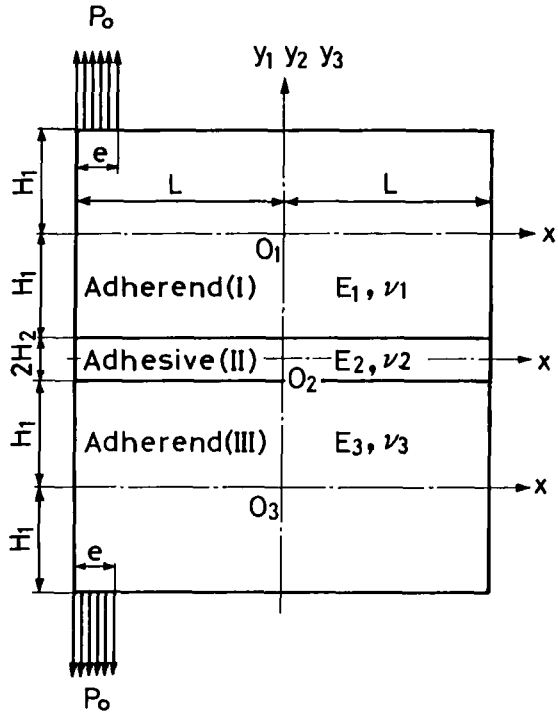

FIGURE 1 Model for analysis of adhesive butt joint of dissimilar adherends subjected to cleavage load.

On the strip (II), i.e., the adhesive (II),

$$\sigma_x^{II} = \tau_{xy}^{II} = 0 \quad (x = \pm L) \tag{1-d}$$

On the strip (III), i.e. the adherend (III),

$$\sigma_x^{III} = \tau_{xy}^{III} = 0 \quad (x = \pm L) \tag{1-e}$$

$$\sigma_y^{III} = \begin{cases} P_0 & (-L \leqq x \leqq -L + e) \\ 0 & (-L + e \leqq x \leqq +L) \end{cases} \quad (y_3 = -H_1) \tag{1-f}$$

$$\tau_{xy}^{III} = 0 \quad (y_3 = -H_1) \tag{1-g}$$

At the interface between the strip (I) and (II), i.e. $(y_1 = -H_1, y_2 = +H_2)$,

$$\sigma_y^{I} = \sigma_y^{II} \quad \text{(1-h)}, \qquad \tau_{xy}^{I} = \tau_{xy}^{II} \tag{1-i}$$

$$\frac{\partial u^{I}}{\partial x} = \frac{\partial u^{II}}{\partial x} \quad \text{(1-j)}, \qquad \frac{\partial v^{I}}{\partial x} = \frac{\partial v^{II}}{\partial x} \tag{1-k}$$

At the interface between the strip (II) and (III), i.e. $(y_2 = -H_2, y_3 = +H_1)$,

$$\sigma_y^{II} = \sigma_y^{III} \quad \text{(1-l)}, \qquad \tau_{xy}^{II} = \tau_{xy}^{III} \tag{1-m}$$

$$\frac{\partial u^{II}}{\partial x} = \frac{\partial u^{III}}{\partial x} \quad \text{(1-n)}, \qquad \frac{\partial v^{II}}{\partial x} = \frac{\partial v^{III}}{\partial x} \tag{1-o}$$

In these equations, σ_x and σ_y denote the normal stresses, τ_{xy} the shear stress, u and v the displacements in x- and y-directions. Suffixes I, II and III denote the strips (I), (II) and (III), respectively.

The stresses and the displacements are expressed as the following equations (2) and (3) by using Airy's stress function χ[12].

$$\sigma_x = \frac{\partial^2 \chi}{\partial y^2}, \quad \sigma_y = \frac{\partial^2 \chi}{\partial x^2}, \quad \tau_{xy} = -\frac{\partial^2 \chi}{\partial x\, \partial y} \tag{2}$$

$$2Gu = -\frac{\partial \chi}{\partial x} + \frac{1}{1+\nu}\frac{\partial \Phi}{\partial y}, \quad 2Gv = -\frac{\partial \chi}{\partial y} + \frac{1}{1+\nu}\frac{\partial \Phi}{\partial x} \tag{3}$$

where

$$\nabla^4 \chi = 0, \quad \nabla^2 \Phi = 0, \quad \nabla^2 \chi = \frac{\partial^2 \Phi}{\partial x\, \partial y}, \quad \nabla^2 = \frac{\partial^2}{\partial x^2} + \frac{\partial^2}{\partial y^2}$$

To analyze each finite strip, the following stress function χ is used in consideration of the boundary conditions.[13]

$$\chi = \chi_1 + \chi_2 + \chi_3 + \chi_4 + \chi_5 + \chi_6 + \chi_7 + \chi_8$$

$$\chi_1 = \frac{A_{01}}{2}x^2 + \sum_{n=1}^{\infty} \frac{\bar{A}_n}{\bar{\Delta}_n \alpha_n^2}[\{\mathrm{sh}(\alpha_n l) + \alpha_n l\, \mathrm{ch}(\alpha_n l)\}\, \mathrm{ch}(\alpha_n x) - \mathrm{sh}(\alpha_n l)\alpha_n x\, \mathrm{sh}(\alpha_n x)]\cos(\alpha_n y) + \sum_{s=1}^{\infty} \frac{\bar{B}_s}{\bar{\Omega}_s \lambda_s^2}[\{\mathrm{sh}(\lambda_s h) + \lambda_s h\, \mathrm{ch}(\lambda_s h)\}\, \mathrm{ch}(\lambda_s y) - \mathrm{sh}(\lambda_s h)\lambda_s y\, \mathrm{sh}(\lambda_s y)]\cos(\lambda_s x)$$

$$\chi_2 = \sum_{n=1}^{\infty} \frac{\bar{\bar{A}}_n}{\bar{\bar{\Delta}}_n \alpha_n^2}[\{\mathrm{ch}(\alpha_n l) + \alpha_n l\, \mathrm{sh}(\alpha_n l)\}\, \mathrm{sh}(\alpha_n x) - \mathrm{ch}(\alpha_n l)\alpha_n x\, \mathrm{ch}(\alpha_n x)]\cos(\alpha_n y) + \sum_{s=1}^{\infty} \frac{\bar{\bar{B}}_n}{\bar{\bar{\Omega}}_s \lambda_s^2}[\{\mathrm{ch}(\lambda_s h) + \lambda_s h\, \mathrm{sh}(\lambda_s h)\}\, \mathrm{sh}(\lambda_s y) - \mathrm{ch}(\lambda_s h)\lambda_s y\, \mathrm{ch}(\lambda_s y)]\cos(\lambda_s x)$$

$$\chi_3 = \sum_{n=1}^{\infty} \frac{\tilde{A}_n}{\tilde{\Delta}_n \alpha_n'^2}[\{\mathrm{sh}(\alpha_n' l) + \alpha_n']\, \mathrm{ch}(\alpha_n' l)\}\, \mathrm{ch}(\alpha_n' x) - \mathrm{sh}(\alpha_n' l)\alpha_n' x\, \mathrm{sh}(\alpha_n' x)]\sin(\alpha_n' y) + \sum_{s=1}^{\infty} \frac{\tilde{B}_s}{\tilde{\Omega}_s \lambda_s'^2}[\{\mathrm{sh}(\lambda_s' h) + \lambda_s' h\, \mathrm{ch}(\lambda_s' h)\}\, \mathrm{ch}(\lambda_s' y) - \mathrm{sh}(\lambda_s' h)\lambda_s' y\, \mathrm{sh}(\lambda_s' y)]\sin(\lambda_s' x)$$

$$\chi_4 = \sum_{n=1}^{\infty} \frac{\tilde{\bar{A}}_n}{\tilde{\bar{\Delta}}_n \alpha_n'^2}[\{\mathrm{ch}(\alpha_n' l) + \alpha_n' l\, \mathrm{sh}(\alpha_n' l)\}\, \mathrm{sh}(\alpha_n' x) - \mathrm{ch}(\alpha_n' l)\alpha_n' x\, \mathrm{ch}(\alpha_n' x)]\sin(\alpha_n' y) + \sum_{s=1}^{\infty} \frac{\tilde{\bar{B}}_s}{\tilde{\bar{\Omega}}_s \lambda_s'^2}[\{\mathrm{ch}(\lambda_s' h) + \lambda_s' h\, \mathrm{sh}(\lambda_s' h)\}\, \mathrm{sh}(\lambda_s' y) - \mathrm{ch}(\lambda_s' h)\lambda_s' y\, \mathrm{ch}(\lambda_s' y)]\sin(\lambda_s' x)$$

$$\chi_5 = \sum_{n=1}^{\infty} \frac{\bar{A}_n'}{\bar{\Delta}_n \alpha_n'^2}\{\mathrm{ch}(\alpha_n' l)\alpha_n' x\, \mathrm{sh}(\alpha_n' x) - \alpha_n' l\, \mathrm{sh}(\alpha_n' l)\, \mathrm{ch}(\alpha_n' x)\}\cos(\alpha_n' y) + \sum_{s=1}^{\infty} \frac{\bar{B}_s'}{\bar{\Omega}_s \lambda_s'^2}\{\mathrm{ch}(\lambda_s' h)\lambda_s' y\, \mathrm{sh}(\lambda_s' y) - \lambda_s' h\, \mathrm{sh}(\lambda_s' h)\, \mathrm{ch}(\lambda_s' y)\}\cos(\lambda_s' x)$$

$$\chi_6 = \sum_{n=1}^{\infty} \frac{\bar{\bar{A}}'_n}{\bar{\bar{\Delta}}_n \alpha'^2_n} \{\mathrm{sh}(\alpha'_n l)\alpha'_n x \,\mathrm{ch}(\alpha'_n x) - \alpha'_n l \,\mathrm{ch}(\alpha'_n l)\,\mathrm{sh}(\alpha'_n x)\} \cos(\alpha'_n y)$$
$$+ \sum_{s=1}^{\infty} \frac{\bar{\bar{B}}'_n}{\bar{\bar{\Omega}}_s \lambda'^2_s} \{\mathrm{sh}(\lambda'_s h)\lambda'_s y \,\mathrm{ch}(\lambda'_s y) - \lambda'_s h \,\mathrm{ch}(\lambda'_s h)\,\mathrm{sh}(\lambda'_s y)\} \cos(\lambda'_s x)$$

$$\chi_7 = \sum_{n=1}^{\infty} \frac{\bar{A}'_n}{\bar{\Delta}_n \alpha_n^2} \{\mathrm{ch}(\alpha_n l)\alpha_n x \,\mathrm{sh}(\alpha_n x) - \alpha_n l \,\mathrm{sh}(\alpha_n l)\,\mathrm{ch}(\alpha_n x)\} \sin(\alpha_n y)$$
$$+ \sum_{s=1}^{\infty} \frac{\bar{B}'_s}{\bar{\Omega}_s \lambda_s^2} \{\mathrm{ch}(\lambda_s h)\lambda_s y \,\mathrm{sh}(\lambda_s y) - \lambda_s h \,\mathrm{sh}(\lambda_s h)\,\mathrm{ch}(\lambda_s y)\} \sin(\lambda_s x)$$

$$\chi_8 = \sum_{n=1}^{\infty} \frac{\bar{\bar{A}}'_n}{\bar{\bar{\Delta}}_n \alpha_n^2} \{\mathrm{sh}(\alpha_n l)\alpha_n x \,\mathrm{ch}(\alpha_n x) - \alpha_n l \,\mathrm{ch}(\alpha_n l)\,\mathrm{sh}(\alpha_n x)\} \sin(\alpha_n y)$$
$$+ \sum_{s=1}^{\infty} \frac{\bar{\bar{B}}'_s}{\bar{\bar{\Omega}}_s \lambda_s^2} \{\mathrm{sh}(\lambda_s h)\lambda_s y \,\mathrm{ch}(\lambda_s y) - \lambda_s h \,\mathrm{ch}(\lambda_s h)\,\mathrm{sh}(\lambda_s y)\} \sin(\lambda_s x) \quad (4)$$

Where,

$$\alpha_n = \frac{n\pi}{h}, \quad \alpha'_n = \frac{2n-1}{2h}\pi, \quad \lambda_s = \frac{s\pi}{l}, \quad \lambda'_s = \frac{2s-1}{2l}\pi \quad (n, s = 1, 2, 3, \ldots)$$

$$\bar{\Delta}_n = \mathrm{sh}(\alpha_n l)\,\mathrm{ch}(\alpha_n l) + \alpha_n l \quad \bar{\Omega}_s = \mathrm{sh}(\lambda_s h)\,\mathrm{ch}(\lambda_s h) + \lambda_s h$$
$$\bar{\bar{\Delta}}_n = \mathrm{sh}(\alpha_n l)\,\mathrm{ch}(\alpha_n l) - \alpha_n l \quad \bar{\bar{\Omega}}_s = \mathrm{sh}(\lambda_s h)\,\mathrm{ch}(\lambda_s h) - \lambda_s h$$
$$\bar{\Delta}_n = \mathrm{sh}(\alpha'_n l)\,\mathrm{ch}(\alpha'_n l) + \alpha'_n l \quad \bar{\Omega}_s = \mathrm{sh}(\lambda'_s h)\,\mathrm{ch}(\lambda'_s h) + \lambda'_s h$$
$$\bar{\bar{\Delta}}_n = \mathrm{sh}(\alpha'_n l)\,\mathrm{ch}(\alpha'_n l) - \alpha'_n l \quad \bar{\bar{\Omega}}_s = \mathrm{sh}(\lambda'_s h)\,\mathrm{ch}(\lambda'_s h) - \lambda'_s h$$

sh = sinh, ch = cosh.

A_{01}, $\bar{A}_n$, $\bar{B}_s$, $\bar{\bar{A}}_n$, $\bar{\bar{B}}_s$, . . . , $\bar{\bar{A}}'_n$, $\bar{\bar{B}}'_s$ $(n, s = 1, 2, 3, \ldots)$ in Eq. (4) are undetermined coefficients obtained from the boundary conditions, expressed in Eq. (1)

The stresses and displacements of each strip are transformed into Fourier series using the stress function, shown in the Appendix. Then, by equating these expressions to the boundary conditions shown in Eq. (1), the infinite simultaneous equations are obtained. In numerical calculations, infinite terms of each series of the above equations are taken as some large finite terms N. Finally, the stresses and the displacements of each strip can be obtained by solving finite simultaneous equations of N terms.

3 EXPERIMENTAL METHOD

Figure 2 shows the dimensions of the adherends (I) and (III) used in the experiments. Three kinds of materials, i.e. carbon steel for structural use (S45C, JIS), aluminum alloy (A1080P, JIS) and brass (C2680P, JIS) were used as the adherends, where their Young's modulus and Poisson's ratio were 206 GPa and 0.3, 72 GPa and 0.33 and 103 GPa and 0.38, respectively. Epoxy resin (Sumitomo 3M Scotch-Weld 1838B/A) was used as the adhesive, where its Young's modulus and Poisson's ratio were 3.6 GPa and 0.38, respectively.

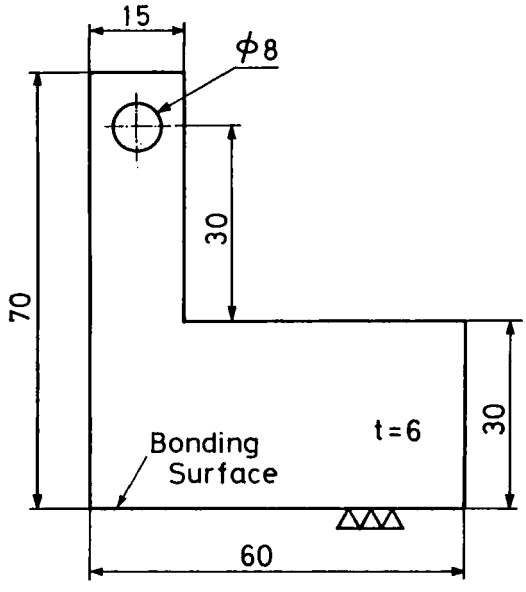

FIGURE 2 Dimensions (mm) of adherends used in experiments.

After two dissimilar adherends were joined by the adhesive, the joint was subjected to a cleavage load using pins inserted in an 8 mm diameter hole. When a load was applied to the joint, the strains induced in adherends (I) and (III) in the y-direction were measured using strain gauges attached to each adherend. Five strain gauges along the length were mounted 2 mm from each interface between the adherend and the adhesive bond.

4 RESULTS

4.1 Numerical results

4.1.1 *Effect of the ratio of Young's modulus* In numerical calculations, the number N of the series is taken as 60. Figure 3 shows the effects of the ratio of Young's modulus of each adherend to that of the adhesive on the stress distributions at each interface between the adherend and the adhesive bond. In these figures, the ordinates indicate the normalized stresses, i.e., normal (σ_y/σ_{ym}) and shear (τ_{xy}/σ_{ym}) stresses, where σ_{ym} is the apparent normal stress obtained by dividing an applied cleavage load by bonded area. The abscissae also indicate the normalized position along the x-direction by the half-width L of the strip. The solid and dotted lines in the figures indicate the stresses at the interfaces between the adhesive (II) and the adherend (I) of the larger Young's modulus, and the adhesive (II) and the adherend (III) of the smaller Young's modulus, respectively.

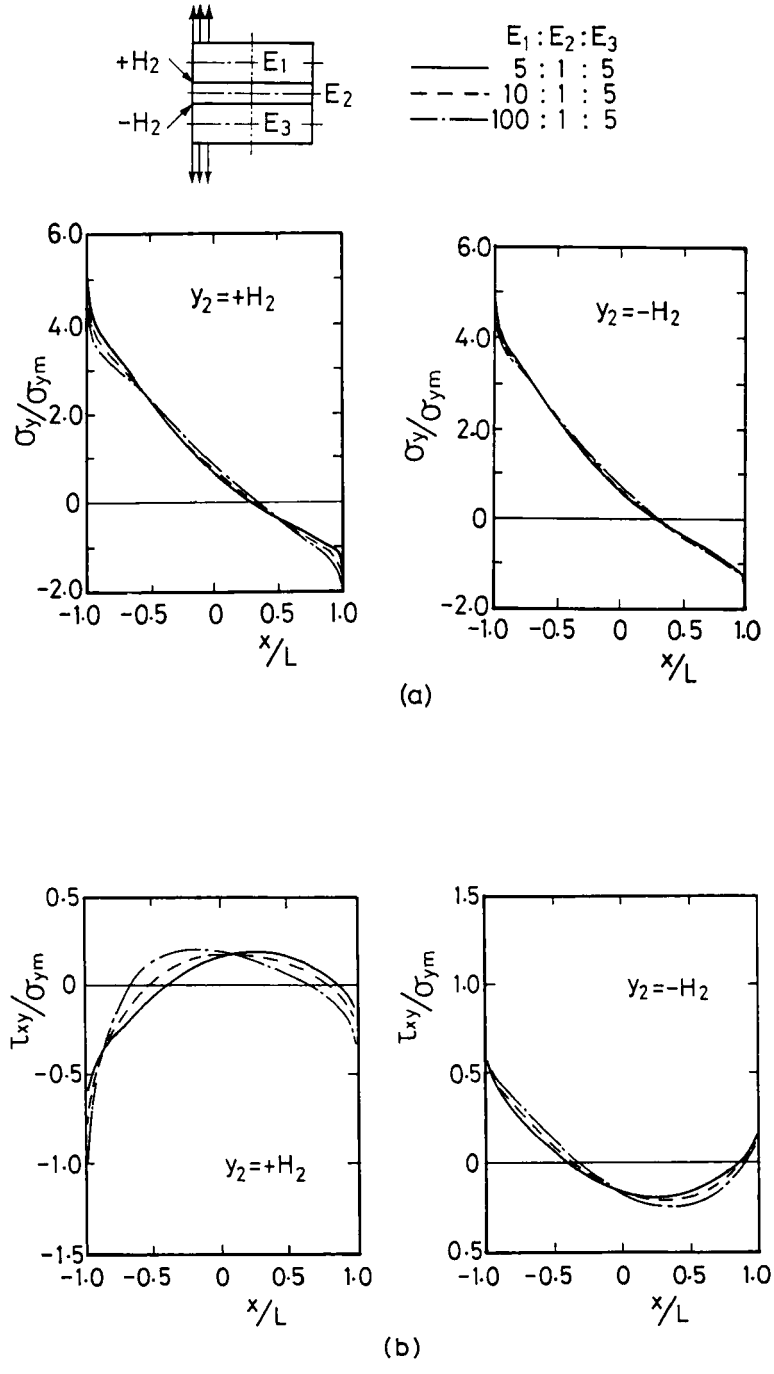

FIGURE 3 Effects of the ratios of Young's modulus among adherends and an adhesive on the stress distributions at each interface of bonding. ($H_1/L = 0.5$, $H_1/H_2 = 2$, $\nu_2 = \nu_2 = \nu_3$, $P_0 = \text{const.}$ ($-1 \leqq x/L \leqq -0.8$)).

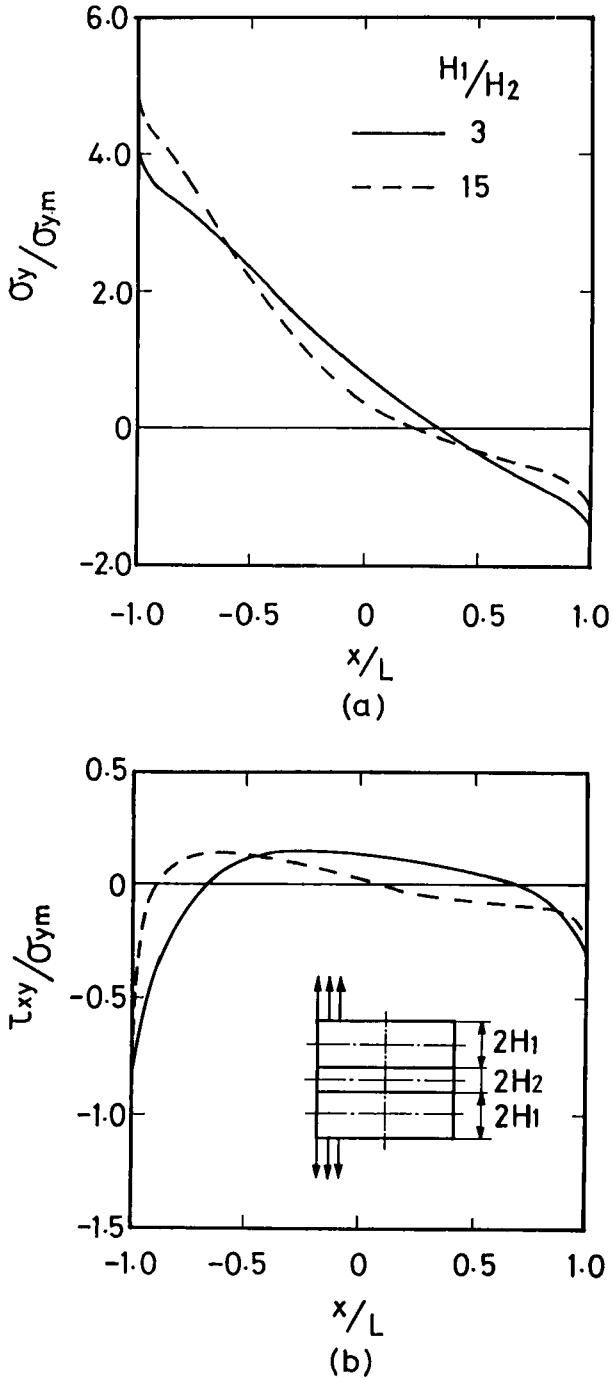

FIGURE 4 Effects of the thickness of adhesive on the stress distributions at interface of bonding. ($y_2 = +H_2$), ($H_1/L = 0.5$, $E_1/E_2 = 25$, $E_3/E_2 = 10$, $\nu_1 = \nu_2 = \nu_3$, $P_0 = \text{const.}$ ($-1 \leqq x/L \leqq -0.8$))

A cleavage load is applied at the extent of $-1.0 \leqq (x/L) \leqq -0.8$. From these figures, it is seen that both stresses are maximal at the edge of the interface on the load application side. Moreover, the stresses at the interface $y_2 = +H_2$ (indicated by the solid lin) between the adherend (I) of the larger Young's modulus and the adhesive (II), increase more steeply at the edge of the interface than those for the dotted line.

In this case, the normal stresses shown in (a) are $4.4\sigma_{ym}$ in both lines near the edge, i.e. at 98% of $-L$ because the stresses are singular at the edge. The shear stresses shown in (b) are $-1.1\sigma_{ym}$ for the solid line and $0.67\sigma_{ym}$ for the dotted line, respectively.

4.1.2 *Effect of the thickness of the adhesive* Figure 4 shows the effects of the thickness of the adhesive bond on the normalized stress distributions σ_y/σ_{ym} and τ_{xy}/σ_{ym} at the interface between the adherend (I) and the adhesive (II), i.e. $y_2 = +H_2$. The solid and the dotted lines in the figures represent relatively thick ($H_1/H_2 = 3$) and relatively thin ($H_1/H_2 = 15$) adhesive bondlines, respectively. From the figures, it is seen that both stresses increase near the edge of the interface on the load application side and, especially with a relatively thin adhesive (indicated by the dotted line), the maximum normal stress is larger than that with a thick adhesive. Concerning the effect of the thickness of the adhesive bond, the result mentioned above is the same as that shown in some studies[14–16] in other types of adhesive joints. The normal stresses shown in (a) are $3.8\sigma_{ym}$ in the solid line and $4.7\sigma_{ym}$ in the dotted line, respectively, near the edge. The shear stresses shown in (b) are $-0.8\sigma_{ym}$ in the solid line and $-0.4\sigma_{ym}$ in the dotted line, respectively.

4.2 Stress distribution near the edge of the interface

The numerical calculations show that the stresses are singular at the edge of the interface as shown in Figures 3 and 4. The stress distributions near the edge are expressed approximately by the following equation.

$$S(r) = Kr^{-\lambda} \tag{5}$$

where,

$S(r)$ = *Normal or shear stress.*
r = Distance from the singular point, i.e. from the edge.
K = Intensity of the stress singularity.
λ = Order of the stress singularity.

Using the parameters K and λ, the characteristic of the stress singularity is evaluated and the parameter λ is determined by the methods demonstrated in Refs 17 and 18. The parameter K is determined in this study by the relationship between the stresses at the close vicinity of the edge and the distance r from the edge in logarithmic scales.

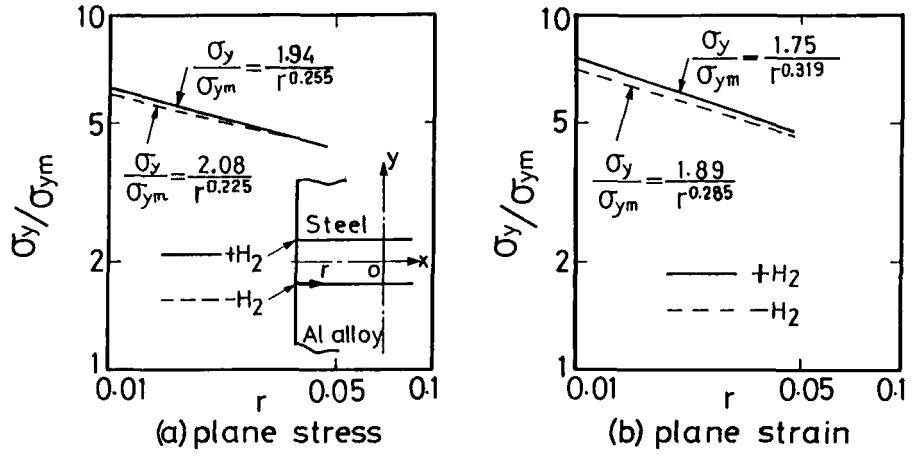

FIGURE 5 Distribution of normal stress near the edge of the interface. ($H_1/L = 0.5$, $P_0 = 0.8$ KN $(-1 \leqq x/L \leqq -0.5)$).

Figure 5 shows the results of two joints in two different plane-states. That is, in Figure 5(a), the joint is in a plane stress state, while in Figure 5(b) the joint is in a plane strain state. The adherends are a steel and an aluminum alloy in both cases. In the figures, the stress $S(r)$ and the distance r are normalized such that $S(r) = \sigma_y/\sigma_{ym}$ and $r = (L + x)/L$. The solid line indicates the stresses at the interface between the steel adherend and the adhesive, and the dotted line at the interface between the adherend of aluminum alloy and the adhesive. From these figures, it is seen that the stress singularity increases at the edge of the interface between the steel adherend and the adhesive. Also, the singularity increases more rapidly in the case of plane strain than in the case of plane stress.

4.3 Comparisons with experimental results

Figure 6 shows a comparison of predicted and measured normal strains ε_y. In this case, the adherends are a carbon steel and an aluminum alloy.

The abscissa denotes the distance from the center of the adherends in the x-direction. The solid line indicates the numerical results for the steel adherend and the dotted line for the aluminum alloy adherend when the cleavage load of 0.8 KN is applied uniformly to the extent of 15 mm from the end of each adherend. In the calculations, the thickness of the adhesive bond ($2H_2$) was measured as 0.04 mm and used in the calculations. The solid circles indicate the experimental results in the case where the adherend is the carbon steel and open circles the aluminum alloy, respectively.

Moreover, in the other combinations of adherends of dissimilar material components, such as steel *vs* brass and brass *vs* aluminum alloy, the same experiments were performed. The calculated results are also satisfactorily consistent with the experimental ones in each case.

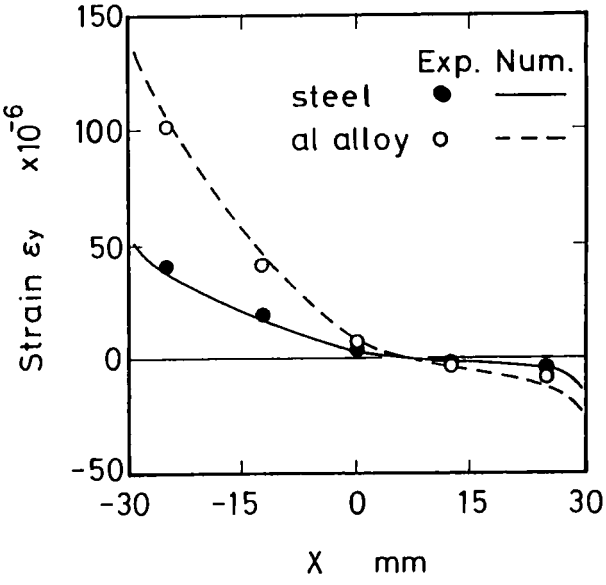

FIGURE 6 Comparison between numerical and experimental results in the case when cleavage load is 0.8 KN. ($y_1 = -13$ mm, $y_3 = +13$ mm).

5 CONCLUSIONS

This paper describes a stress analysis of an adhesive butt joint in which two dissimilar adherends are joined and subjected to a cleavage load.

The effects of the ratio of Young's modulus of the adherends to that of the adhesive and of the thickness of the adhesive bond on the stress distributions of the joint were examined by the numerical calculations. Some experiments were performed for verification. The results obtained are as follows:

1) The stress distributions and the displacements of the adhesive butt joint in which the two dissimilar adherends are joined and subjected to a cleavage load are analyzed using the two-dimensional theory of elasticity.

2) The normal and the shear stresses become maximal at the edge of the interface on the load application side between the adherends and the adhesive bond. Both stresses increase near the edge of the interface between the adherend of the larger Young's modulus and the adhesive bond.

3) The maximum normal stress increases with a decrease in the thickness of the adhesive bond.

4) The behavior of the stress singularity near the edge of the interface was evaluated quantitatively for both the plane stress case and the plane strain case. Plane strain conditions result in a more severe stress singularity near the joint edge than in the plane stress case.

5) The strain distributions of the adherends near the interfaces were measured.

The numerical results obtained from this stress analysis are fairly consistent with experimental measurements.

References

1. R. M. Baker and F. Hatt, *AIAA Journal*, **11**, 1650 (1973).
2. J. K. Sen and R. M. Jones, *AIAA Journal*, **18**, 1237 (1980).
3. R. D. Adams, J. Coppendale and N. A. Peppiatt, *J. Strain Analysis*, **13**, 1 (1978).
4. F. Erdogan and M. Ratwani, *J. Composite Materials*, **5**, 378 (1971).
5. T. Wah, *Int. J. Solids and Structures*, **12**, 491 (1976).
6. J. W. Renton and J. R. Vinson, *J. Appl. Mechanics*, **44**, 101 (1977).
7. D. Chen and S. Cheng, *J. Appl. Mechanics*, **50**, 109 (1983).
8. Y. Nakano, T. Sawa and S. Arai, *Int. J. Adhesion and Adhesives*, **9**, 2 (1989).
9. K. Temma and T. Sawa, *Int. J. Adhesion and Adhesives*, (in printing).
10. Y. Nakano, K. Temma and T. Sawa, *JSME Int. J. ser. 1*, **31**, 3 (1988).
11. T. Sawa, K. Temma and Y. Tsunoda, *Int. J. Adhesion and Adhesives*, **9**, 3 (1989).
12. S. P. Timoshenko and J. N. Goodier, *Theory of Elasticity*, 3rd ed. (McGraw-Hill, New York, 1970), pp. 31–32.
13. T. Sawa, Y. Nakano and K. Temma, *J. Adhesion*, **24**, 1 (1987).
14. A. N. Gent, *J. Polym. Sci.* **A2**, 283 (1974).
15. D. L. Hunston, A. J. Kinloch, S. J. Shaw and S. S. Wang, in *Adhesive Joints*, K. L. Mittal, Ed. (Plenum Press, New York, 1982), pp. 789–808.
16. A. J. Kinloch, *Adhesion and Adhesives*, 1st. ed. (Chapman and Hall, London and New York, 1987), pp. 206–214.
17. T. Hattori, S. Sakata and T. Watanabe, *Proc. The Annual Winter Meeting of ASME*, pp. 43 (1988).
18. D. B. Body, *J. Appl. Mechanics*, **38**, 377 (1971).

Appendix

$$\sigma_x = -\sum_{n=1}^{\infty} \frac{\bar{A}_n}{\bar{\Delta}_n}[\{\mathrm{sh}(\alpha_n l) + \alpha_n l\,\mathrm{ch}(\alpha_n l)\}\,\mathrm{ch}(\alpha_n x) - \mathrm{sh}(\alpha_n l)\alpha_n x\,\mathrm{sh}(\alpha_n x)]\cos(\alpha_n y)$$

$$-\sum_{s=1}^{\infty} \frac{\bar{B}_s}{\bar{\Omega}_s}[\{\mathrm{sh}(\lambda_s h) - \lambda_s h\,\mathrm{ch}(\lambda_s h)\}\,\mathrm{ch}(\lambda_s y) + \mathrm{sh}(\lambda_s h)\lambda_s y\,\mathrm{sh}(\lambda_s y)]\cos(\lambda_s x)$$

$$-\sum_{n=1}^{\infty} \frac{\bar{\bar{A}}_n}{\bar{\bar{\Delta}}_n}[\{\mathrm{ch}(\alpha_n l) + \alpha_n l\,\mathrm{sh}(\alpha_n l)\}\,\mathrm{sh}(\alpha_n x) - \mathrm{ch}(\alpha_n l)\alpha_n x\,\mathrm{ch}(\alpha_n x)]\cos(\alpha_n y)$$

$$-\sum_{s=1}^{\infty} \frac{\bar{\bar{B}}_s}{\bar{\bar{\Omega}}_s}[\{\mathrm{ch}(\lambda_s h) - \lambda_s h\,\mathrm{sh}(\lambda_s h)\}\,\mathrm{sh}(\lambda_s y) + \mathrm{ch}(\lambda_s h)\lambda_s y\,\mathrm{ch}(\lambda_s y)]\cos(\lambda_s x)$$

$$-\sum_{n=1}^{\infty} \frac{\tilde{A}_n}{\tilde{\Delta}_n}[\{\mathrm{sh}(\alpha'_n l) + \alpha'_n l\,\mathrm{ch}(\alpha'_n l)\}\,\mathrm{ch}(\alpha'_n x) - \mathrm{sh}(\alpha'_n l)\alpha'_n x\,\mathrm{sh}(\alpha'_n x)]\sin(\alpha'_n y)$$

$$-\sum_{s=1}^{\infty} \frac{\tilde{B}_s}{\tilde{\Omega}_s}[\{\mathrm{sh}(\lambda'_s h) - \lambda'_s h\,\mathrm{ch}(\lambda'_s h)\}\,\mathrm{ch}(\lambda'_s y) + \mathrm{sh}(\lambda'_s h)\lambda'_s y\,\mathrm{sh}(\lambda'_s y)]\sin(\lambda'_s x)$$

$$-\sum_{n=1}^{\infty} \frac{\tilde{\bar{A}}_n}{\tilde{\bar{\Delta}}_n}[\{\mathrm{ch}(\alpha'_n l) + \alpha'_n l\,\mathrm{sh}(\alpha'_n)\}\,\mathrm{sh}(\alpha'_n x) - \mathrm{ch}(\alpha'_n l)\alpha'_n x\,\mathrm{ch}(\alpha'_n x)]\sin(\alpha'_n y)$$

$$-\sum_{s=1}^{\infty} \frac{\tilde{\bar{B}}_s}{\tilde{\bar{\Omega}}_s}[\{\mathrm{ch}(\lambda'_s h) - \lambda'_s h\,\mathrm{sh}(\lambda'_s h)\}\,\mathrm{sh}(\lambda'_s y) + \mathrm{ch}(\lambda'_s h)\lambda'_s y\,\mathrm{ch}(\lambda'_s y)]\sin(\lambda'_s x)$$

$$+\sum_{n=1}^{\infty}\frac{\bar{A}'_n}{\bar{\Delta}_n}\{\alpha'_n l\,\mathrm{sh}(\alpha'_n l)\,\mathrm{ch}(\alpha'_n x)-\mathrm{ch}(\alpha'_n l)\alpha'_n x\,\mathrm{sh}(\alpha'_n x)\}\cos(\alpha'_n y)$$

$$+\sum_{s=1}^{\infty}\frac{\bar{B}'_s}{\bar{\Omega}_s}[\{2\mathrm{ch}(\lambda'_s h)-\lambda'_s h\,\mathrm{sh}(\lambda'_s h)\}\,\mathrm{ch}(\lambda'_s y)+\mathrm{ch}(\lambda'_s h)\lambda'_s y\,\mathrm{sh}(\lambda'_s y)]\cos(\lambda'_s x)$$

$$+\sum_{n=1}^{\infty}\frac{\bar{\bar{A}}'_n}{\bar{\bar{\Delta}}_n}\{\alpha'_n l\,\mathrm{ch}(\alpha'_n l)\,\mathrm{sh}(\alpha'_n x)-\mathrm{sh}(\alpha'_n l)\alpha'_n x\,\mathrm{ch}(\alpha'_n x)\}\cos(\alpha'_n y)$$

$$+\sum_{s=1}^{\infty}\frac{\bar{\bar{B}}'_s}{\bar{\bar{\Omega}}_s}[\{2\mathrm{sh}(\lambda'_s h)-\lambda'_s h\,\mathrm{ch}(\lambda'_s h)\}\,\mathrm{sh}(\lambda'_s y)+\mathrm{sh}(\lambda'_s h)\lambda'_s y\,\mathrm{ch}(\lambda'_s y)]\cos(\lambda'_s x)$$

$$+\sum_{n=1}^{\infty}\frac{\bar{A}'_n}{\bar{\Delta}_n}\{\alpha_n l\,\mathrm{sh}(\alpha_n l)\,\mathrm{ch}(\alpha_n x)-\mathrm{ch}(\alpha_n l)\alpha_n x\,\mathrm{sh}(\alpha_n x)\}\sin(\alpha_n y)$$

$$+\sum_{s=1}^{\infty}\frac{\bar{B}'_s}{\bar{\Omega}_s}[\{2\mathrm{ch}(\lambda_s h)-\lambda_s h\,\mathrm{sh}(\lambda_s h)\}\,\mathrm{ch}(\lambda_s y)+\mathrm{ch}(\lambda_s h)\lambda_s y\,\mathrm{sh}(\lambda_s y)]\sin(\lambda_s x)$$

$$+\sum_{n=1}^{\infty}\frac{\bar{\bar{A}}'_n}{\bar{\bar{\Delta}}_n}\{\alpha_n l\,\mathrm{ch}(\alpha_n l)\,\mathrm{sh}(\alpha_n x)-\mathrm{sh}(\alpha_n l)\alpha_n x\,\mathrm{ch}(\alpha_n x)\}\sin(\alpha_n y)$$

$$+\sum_{s=1}^{\infty}\frac{\bar{\bar{B}}'_s}{\bar{\bar{\Omega}}_s}[\{2\mathrm{sh}\,(\lambda_s h)-\lambda_s h\,\mathrm{ch}(\lambda_s h)\}\,\mathrm{sh}(\lambda_s y)+\mathrm{sh}(\lambda_s h)\lambda_s y\,\mathrm{ch}(\lambda_s y)]\sin(\lambda_s x)$$

$$\sigma_y = A_{01}$$

$$-\sum_{n=1}^{\infty}\frac{\bar{A}_n}{\bar{\Delta}_n}[\{\mathrm{sh}(\alpha_n l)-\alpha_n l\,\mathrm{ch}(\alpha_n l)\}\,\mathrm{ch}(\alpha_n x)+\mathrm{sh}(\alpha_n l)\alpha_n x\,\mathrm{sh}(\alpha_n x)]\cos(\alpha_n y)$$

$$-\sum_{s=1}^{\infty}\frac{\bar{B}_s}{\bar{\Omega}_s}[\{\mathrm{sh}(\lambda_s h)+\lambda_s h\,\mathrm{ch}(\lambda_s h)\}\,\mathrm{ch}(\lambda_s y)-\mathrm{sh}(\lambda_s h)\lambda_s y\,\mathrm{sh}(\lambda_s y)]\cos(\lambda_s x)$$

$$-\sum_{n=1}^{\infty}\frac{\bar{\bar{A}}_n}{\bar{\bar{\Delta}}_n}[\{\mathrm{ch}(\alpha_n l)-\alpha_n l\,\mathrm{sh}(\alpha_n l)\}\,\mathrm{sh}(\alpha_n x)+\mathrm{ch}(\alpha_n l)\alpha_n x\,\mathrm{ch}(\alpha_n x)]\cos(\alpha_n y)$$

$$-\sum_{s=1}^{\infty}\frac{\bar{\bar{B}}_s}{\bar{\bar{\Omega}}_s}[\{\mathrm{ch}(\lambda_s h)+\lambda_s h\,\mathrm{sh}(\lambda_s h)\}\,\mathrm{sh}(\lambda_s y)-\mathrm{ch}(\lambda_s h)\lambda_s y\,\mathrm{ch}(\lambda_s y)]\cos(\lambda_s x)$$

$$-\sum_{n=1}^{\infty}\frac{\bar{A}_n}{\bar{\Delta}_n}[\{\mathrm{sh}(\alpha'_n l)-\alpha'_n l\,\mathrm{ch}(\alpha'_n l)\}\,\mathrm{ch}(\alpha'_n x)+\mathrm{sh}(\alpha'_n l)\alpha'_n x\,\mathrm{sh}(\alpha'_n x)]\sin(\alpha'_n y)$$

$$-\sum_{s=1}^{\infty}\frac{\bar{B}_s}{\bar{\Omega}_s}[\{\mathrm{sh}(\lambda'_s h)+\lambda'_s h\,\mathrm{ch}(\lambda'_s h)\}\,\mathrm{ch}(\lambda'_s y)-\mathrm{sh}(\lambda'_s h)\lambda'_s y\,\mathrm{sh}(\lambda'_s y)]\sin(\lambda'_s x)$$

$$-\sum_{n=1}^{\infty}\frac{\bar{\bar{A}}_n}{\bar{\bar{\Delta}}_n}[\{\mathrm{ch}(\alpha'_n l)-\alpha'_n l\,\mathrm{sh}(\alpha'_n l)\}\,\mathrm{sh}(\alpha'_n x)+\mathrm{ch}(\alpha'_n l)\alpha'_n x\,\mathrm{ch}(\alpha'_n x)]\sin(\alpha'_n y)$$

$$-\sum_{s=1}^{\infty}\frac{\bar{\bar{B}}_s}{\bar{\bar{\Omega}}_s}[\{\mathrm{ch}(\lambda'_s h)+\lambda'_s h\,\mathrm{sh}(\lambda'_s h)\}\,\mathrm{sh}(\lambda'_s y)-\mathrm{ch}(\lambda'_s h)\lambda'_s y\,\mathrm{ch}(\lambda'_s y)]\sin(\lambda'_s x)$$

$$+\sum_{s=1}^{\infty}\frac{\bar{A}'_n}{\bar{\Delta}_n}[\{2\mathrm{ch}(\alpha'_n l)-\alpha'_n l\,\mathrm{sh}(\alpha'_n l)\}\,\mathrm{ch}(\alpha'_n x)+\mathrm{ch}(\alpha'_n l)\alpha'_n x\,\mathrm{sh}(\alpha'_n x)]\cos(\alpha'_n y)$$

$$+\sum_{s=1}^{\infty}\frac{\bar{B}'_s}{\bar{\Omega}_s}\{\lambda'_s h\,\mathrm{sh}(\lambda'_s h)\,\mathrm{ch}(\lambda'_s y)-\mathrm{ch}(\lambda'_s h)\lambda'_s y\,\mathrm{sh}(\lambda'_s y)\}\cos(\lambda'_s x)$$

$$+\sum_{n=1}^{\infty}\frac{\bar{\bar{A}}'_n}{\bar{\bar{\Delta}}_n}[\{2\mathrm{sh}(\alpha'_n l)-\alpha'_n l\,\mathrm{ch}(\alpha'_n l)\}\,\mathrm{sh}(\alpha'_n x)+\mathrm{sh}(\alpha'_n l)\alpha'_n x\,\mathrm{ch}(\alpha'_n x)]\cos(\alpha'_n y)$$

$$+\sum_{s=1}^{\infty}\frac{\bar{\bar{B}}'_s}{\bar{\bar{\Omega}}_s}\{\lambda'_s h\,\mathrm{ch}(\lambda'_s h)\,\mathrm{sh}(\lambda'_s y)-\mathrm{sh}(\lambda'_s h)\lambda'_s y\,\mathrm{ch}(\lambda'_s y)\}\cos(\lambda'_s x)$$

$$+\sum_{n=1}^{\infty}\frac{\tilde{A}'_n}{\tilde{\Delta}_n}[\{2\mathrm{ch}(\alpha_n l)-\alpha_n l\,\mathrm{sh}(\alpha_n l)\}\,\mathrm{ch}(\alpha_n x)+\mathrm{ch}(\alpha_n l)\alpha_n x\,\mathrm{sh}(\alpha_n x)]\sin(\alpha_n y)$$

$$+\sum_{s=1}^{\infty}\frac{\tilde{B}'_s}{\tilde{\Omega}_s}\{\lambda_s h\,\mathrm{sh}(\lambda_s h)\,\mathrm{ch}(\lambda_s y)-\mathrm{ch}(\lambda_s h)\lambda_s y\,\mathrm{sh}(\lambda_s y)\}\sin(\lambda_s x)$$

$$+\sum_{n=1}^{\infty}\frac{\bar{\tilde{A}}'_n}{\bar{\tilde{\Delta}}_n}[\{2\mathrm{sh}(\alpha_n l)-\alpha_n l\,\mathrm{ch}(\alpha_n l)\}\,\mathrm{sh}(\alpha_n x)+\mathrm{sh}(\alpha_n l)\alpha_n x\,\mathrm{ch}(\alpha_n x)]\,\mathrm{sin}(\alpha_n y)$$

$$+\sum_{s=1}^{\infty}\frac{\bar{\tilde{B}}'_s}{\bar{\tilde{\Omega}}_s}\{\lambda_s h\,\mathrm{ch}(\lambda_s h)\,\mathrm{sh}(\lambda_s y)-\mathrm{sh}(\lambda_s h)\lambda_s y\,\mathrm{ch}(\lambda_s y)\}\sin(\lambda_s x)$$

$$\tau_{xy}=\sum_{n=1}^{\infty}\frac{\bar{A}_n}{\bar{\Delta}_n}\{\alpha_n l\,\mathrm{ch}(\alpha_n l)\,\mathrm{sh}(\alpha_n x)-\mathrm{sh}(\alpha_n l)\alpha_n x\,\mathrm{ch}(\alpha_n x)\}\sin(\alpha_n y)$$

$$+\sum_{s=1}^{\infty}\frac{\bar{B}_s}{\bar{\Omega}_s}\{\lambda_s h\,\mathrm{ch}(\lambda_s h)\,\mathrm{sh}(\lambda_s y)-\mathrm{sh}(\lambda_s h)\lambda_s y\,\mathrm{ch}(\lambda_s y)\}\sin(\lambda_s x)$$

$$+\sum_{n=1}^{\infty}\frac{\bar{\bar{A}}_n}{\bar{\bar{\Delta}}_n}\{\alpha_n l\,\mathrm{sh}(\alpha_n l)\,\mathrm{ch}(\alpha_n x)-\mathrm{ch}(\alpha_n l)\alpha_n x\,\mathrm{sh}(\alpha_n x)\}\sin(\alpha_n y)$$

$$+\sum_{s=1}^{\infty}\frac{\bar{\bar{B}}_s}{\bar{\bar{\Omega}}_s}\{\lambda_s h\,\mathrm{sh}(\lambda_s h)\,\mathrm{ch}(\lambda_s y)-\mathrm{ch}(\lambda_s h)\lambda_s y\,\mathrm{sh}(\lambda_s y)\}\sin(\lambda_s x)$$

$$-\sum_{n=1}^{\infty}\frac{\tilde{A}_n}{\tilde{\Delta}_n}\{\alpha'_n l\,\mathrm{ch}(\alpha'_n l)\,\mathrm{sh}(\alpha'_n x)-\mathrm{sh}(\alpha'_n l)\alpha'_n x\,\mathrm{ch}(\alpha'_n x)\}\cos(\alpha'_n y)$$

$$-\sum_{s=1}^{\infty}\frac{\tilde{B}_s}{\tilde{\Omega}_s}\{\lambda'_s h\,\mathrm{ch}(\lambda'_s h)\,\mathrm{sh}(\lambda'_s y)-\mathrm{sh}(\lambda'_s h)\lambda'_s y\,\mathrm{ch}(\lambda'_s y)\}\cos(\lambda'_s x)$$

$$-\sum_{n=1}^{\infty}\frac{\bar{\tilde{A}}_n}{\bar{\tilde{\Delta}}_n}\{\alpha'_n l\,\mathrm{sh}(\alpha'_n l)\,\mathrm{ch}(\alpha'_n x)-\mathrm{ch}(\alpha'_n l)\alpha'_n x\,\mathrm{sh}(\alpha'_n x)\}\cos(\alpha'_n y)$$

$$-\sum_{s=1}^{\infty}\frac{\bar{\tilde{B}}_s}{\bar{\tilde{\Omega}}_s}\{\lambda'_s h\,\mathrm{sh}(\lambda'_s h)\,\mathrm{ch}(\lambda'_s y)-\mathrm{ch}(\lambda'_s h)\lambda'_s y\,\mathrm{sh}(\lambda'_s y)\}\cos(\lambda'_s x)$$

$$+\sum_{n=1}^{\infty}\frac{\bar{A}'_n}{\bar{\Delta}_n}[\{\mathrm{ch}(\alpha'_n l)-\alpha'_n l\,\mathrm{sh}(\alpha'_n l)\}\,\mathrm{sh}(\alpha'_n x)+\mathrm{ch}(\alpha'_n l)\alpha'_n x\,\mathrm{ch}(\alpha'_n x)]\sin(\alpha'_n y)$$

$$+\sum_{s=1}^{\infty}\frac{\bar{B}'_s}{\bar{\Omega}_s}[\{\mathrm{ch}(\lambda'_s h)-\lambda'_s h\,\mathrm{sh}(\lambda'_s h)\}\,\mathrm{sh}(\lambda'_s y)+\mathrm{ch}(\lambda'_s h)\lambda'_s y\,\mathrm{ch}(\lambda'_s y)]\sin(\lambda'_s x)$$

$$+\sum_{n=1}^{\infty}\frac{\bar{\bar{A}}'_n}{\bar{\bar{\Delta}}_n}[\{\mathrm{sh}(\alpha'_n l)-\alpha'_n l\,\mathrm{ch}(\alpha'_n l)\}\,\mathrm{ch}(\alpha'_n x)+\mathrm{sh}(\alpha'_n l)\alpha'_n x\,\mathrm{sh}(\alpha'_n x)]\sin(\alpha'_n y)$$

$$+\sum_{s=1}^{\infty}\frac{\bar{\bar{B}}'_s}{\bar{\bar{\Omega}}_s}[\{\mathrm{sh}(\lambda'_s h)-\lambda'_s h\,\mathrm{ch}(\lambda'_s h)\}\,\mathrm{ch}(\lambda'_s y)+\mathrm{sh}(\lambda'_s h)\lambda'_s y\,\mathrm{sh}(\lambda'_s y)]\sin(\lambda'_s x)$$

$$-\sum_{n=1}^{\infty}\frac{\tilde{A}'_n}{\bar{\Delta}_n}[\{\mathrm{ch}(\alpha_n l)-\alpha_n l\,\mathrm{sh}(\alpha_n l)\}\,\mathrm{sh}(\alpha_n x)+\mathrm{ch}(\alpha_n l)\alpha_n x\,\mathrm{ch}(\alpha_n x)]\cos(\alpha_n y)$$

$$-\sum_{n=1}^{\infty}\frac{\tilde{B}'_s}{\bar{\Omega}_s}[\{\mathrm{ch}(\lambda_s h)-\lambda_s h\,\mathrm{sh}(\lambda_s h)\}\,\mathrm{sh}(\lambda_s y)+\mathrm{ch}(\lambda_s h)\lambda_s y\,\mathrm{ch}(\lambda_s y)]\cos(\lambda_s x)$$

$$-\sum_{n=1}^{\infty}\frac{\bar{\tilde{A}}'_n}{\bar{\Delta}_n}[\{\mathrm{sh}(\alpha_n l)-\alpha_n l\,\mathrm{ch}(\alpha_n l)\}\,\mathrm{ch}(\alpha_n x)+\mathrm{sh}(\alpha_n l)\alpha_n x\,\mathrm{sh}(\alpha_n x)]\cos(\alpha_n y)$$

$$-\sum_{n=1}^{\infty}\frac{\bar{\bar{B}}'_s}{\bar{\bar{\Omega}}_s}[\{\mathrm{sh}(\lambda_s h)-\lambda_s h\,\mathrm{ch}(\lambda_s h)\}\,\mathrm{ch}(\lambda_s y)+\mathrm{sh}(\lambda_s h)\lambda_s y\,\mathrm{sh}(\lambda_s y)]\cos(\lambda_s x)$$